



Spatio-temporal evolution of coastlines of sand-barrier lagoons over 26 years through historic Landsat imagery in Lingshui County, Hainan Province, China

Peihong Jia^{1,2,3} · Yinglong Zhang⁴ · Wei Xu³ · Zhen Xia⁵ · Chongqing Zhong^{1,2,3} · Yong Yin^{1,2,3}

Received: 19 January 2018 / Revised: 10 September 2018 / Accepted: 11 September 2018 / Published online: 25 October 2018
© Springer Nature B.V. 2018

Abstract

Coastlines of sand-barrier lagoons have provided significant locations for coastal economic development as has frequently occurred along the eastern coast of Hainan Island in southern China. Here, increased levels of human activity have greatly destabilized this ecosystem, subjecting it to major damage. The present study used innovative technology to classify and evaluate six phases of overlapping coastlines in Li'an and Xincun Lagoons in Lingshui County in southeastern Hainan Island between 1987 and 2013. This included the retrieval and integrated analysis of remote sensing images that was combined with data related to ocean dynamics and bathymetric surveys. Average historic high-tide lines were acquired by extracting humidity parameters from images using the Kauth-Thomas Transformation. Variations in the position and length of multiple coastlines were analyzed using GIS with a mathematical and statistical approach. The lengths of anthropogenic coastlines increased by 50% and moved seawards by 94.04 m in Li'an and 102.56 m in Xincun. Meanwhile, the areas in the Xincun and Li'an Lagoons decreased from 21.17 km² to 19.43 km² (−8.2%) and 9.94 km² to 7.92 km² (20.3%), respectively. Extensive human activity along the coastlines, such as saltwater aquaculture and farming, salt plant, and land reclamation, have profoundly altered the sedimentary geomorphology, local hydrodynamics, and the ecosystem itself. Consequently, the coastlines in Xincun and Li'an Lagoons in this newly designated pilot tourism city became vulnerable to modification. This research fills a critical gap related to the evolution of historical coastlines and provides an inventory of coastlines in support of coastal management.

Keywords Sand-barrier lagoon · Coastlines evolution · Kauth-Thomas transformation · Humidity component threshold · Lingshui County in southeastern Hainan Island

Introduction

A typical sand-barrier tidal-inlet lagoon is composed of three elements: the tidal basin (lagoon), sand-barrier sediments

(sand-barrier and barrier-island landforms) and tidal inlets through which the lagoons exchange water with the outer sea (Gao and Collins 1994). As remnants of Holocene landforms, these lagoons have special geomorphological characters and developmental histories, representing some of the world's most vulnerable landforms (Anthony and Blivi 1999; Jia et al 2016). Sixty percent of China's coastline and 13% of the world's coastline comprise sand-barrier lagoons; globally, these landforms have attracted intense interest from the research community as part of an analysis of human-ocean interactions (Li et al 2014).

Sand-barrier lagoons, as a special landform that spans both sea and land, not only provide abundant resources, such as land, mineral salt, diverse assemblages of species, sea ports, tourist attractions and scenic views; they also play an important role in coastal protection, flood prevention, air purification, river-runoff control, groundwater recharge and the regulation of the regional fresh water balance, while supporting biodiversity and providing an aesthetically

✉ Peihong Jia
jiaph@nju.edu.cn

¹ School of Geography and Ocean Science, Nanjing University, Nanjing 210023, China

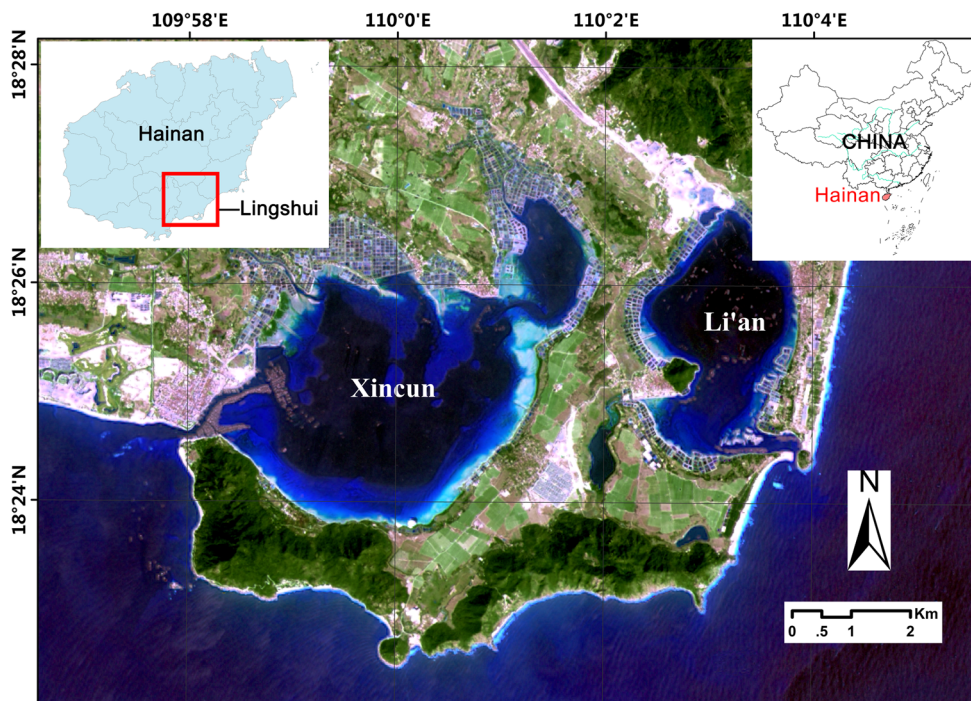
² Key Laboratory of Coast and Island Development (Nanjing University), Ministry of Education, Nanjing 210023, China

³ Collaborative Innovation Center of South China Sea Studies, Nanjing University, Nanjing 210023, China

⁴ Virginia Institute of Marine Science, College of William & Mary, VA 23062, USA

⁵ Guangzhou Marine Geological Survey, Guangzhou 510760, China

Fig. 1 Study area and locations of Li'an and Xincun Lagoons. Inset maps (right) show the location of Hainan Island within China and (left) of the Lingshui County within Hainan Island



pleasing environment (Gao et al. 2016). Meanwhile, sand-barrier lagoons also serve as typical but vulnerable areas situated at the interface between human activities and the ocean. Excessive anthropogenic activity, such as over-exploitation through fish culture, land reclamation, dam building, salt industry activity, and harbor construction, alters the length and landforms of coastlines, thus damaging the physical and ecological functions of lagoons; this may even lead to marine disasters, such as flooding, storm surges, coastline erosion, huge waves, red tides, and the deterioration of water quality. These disasters damaged the marine and agricultural economy, and sometimes cause the irreversible degradation of the lagoon environment, even causing its speedy demise (Gao and Collins 1994).

Xincun and Li'an form a double sand-barrier lagoon system with a large belly and small inlet; these two lagoons lie adjacent to each other and form a typical tide-inlet sedimentary system located in Lingshui County, southeast Hainan Island in southern China. Over the past several decades years, their spatial and

landform coastal patterns have undergone great changes because of extensive anthropogenic activity, such as land reclamation, harbor construction, and fish farming (Chinese Compilation Committee of Embayment 1999). In 2009, this area of extreme coastal and scenic beauty was selected as a new coastal city featuring international tourism for the next 10 years by the Hainan Provincial Government; in addition, the area serves as part of the Free Trade Zone of Hainan Island, which is in turn a part of a new national project. Therefore, an urgent need exists to understand the evolution of its geomorphological environment and to learn how to re-invigorate the coastline.

Remote sensing (RS) images are commonly used to extract information about coastlines due to their use as a long-term data source and ease of access (Liu et al. 2013). Frihy et al. (1998) extracted land and water boundaries to analyze changes in the coastline and coastal erosion through an unsupervised classification method. Ryu et al. (2002) extracted intertidal coastlines of Gomso Bay in Korea while

Table 1 Parameters of data sources

Name	Format	Quantity	Year	Scale	Description
RS images	Landsat TM Landsat ETM+ Landsat OLI	8	1987–2013	30 m	USGS
Bathymetry data	Digital vector data (AutoCAD DWG)	1	2011	–	Surveying on site
Land terrain data	Digital vector data (AutoCAD DWG)	1	2011	1:1000	Surveying on site
Tidal level data	Excel data	4	2013	–	Surveying on site

Three of eight phrases RS images captured in 2013; tide data collected on Aug. 1, to Sep. 1, 2013

combining terrain data on tidal flats with sedimentary particle size and soil moisture data through RS data from Landsat Thematic Mapper (TM) and the Advanced Spaceborne Thermal Emission and Reflection Radiometer remote sensing instruments. Feng et al. (2007) extracted the coastlines of the Yellow River delta with the wavelet transform method. Liu et al. (2004), using eastern Jiangsu Province as an example, extracted mudflat terrain quickly from Landsat 7 Enhanced TM+ (ETM+) imagery by analyzing spectral characters of typical samples and by establishing a recognition function to differentiate different mud tidal flat features. Wang et al. (2013) studied the coastline evolution of Rushan Bay, Shandong Province, China, in the past 40 years using a RS geomorphic interpretation method. However, little research has been conducted on historic coastline extraction and evaluation in a tropical sand-barrier lagoon area with RS imagery.

The present study employed an innovative and integrated technological method to combine the spatio-temporal analysis of a Geographic Information System (GIS), long-term retrieval of RS images, ocean hydrodynamic data, and bathymetry modeling to extract coastlines for 6-year periods in Li'an and Xincun Lagoons in Lingshui County, Hainan Island, between 1987 and 2013. Meanwhile, the average historical high-tide lines were acquired by extracting humidity parameters from the images by the method of Kauth-Thomas (K-T) Transformation. Therefore, this study fills a critical knowledge gap on the evolution of coastlines, where historic tidal data are lacking. With this new technology, the present study analyzed the change of coastlines over multi-year spans and investigated when and how much the coastlines moved on spatio-temporal scales and to what extent anthropogenic activity have affected them. The research not only provides the fundamental scientific methods and technologies needed to further analyze hydrodynamic, geomorphological, and environmental processes but also provides data that will help local governments build a coastline inventory and apply scientifically sound management practices in order to strike a balance between preserving coastline resources and spurring economic development.

Material

Research area

The research area is located in Lingshui County, southeast of Hainan Island (18°22'–47'N, 109°45'E–110°08'E; Fig. 1), and features two lagoons with very interesting and unique physical scenery as well as special marine culture communities and the Danjia pontoons, which are controlled by diurnal tides. Villages of fishermen have lived and worked on the Danjia pontoons in the lagoons for generations. The two lagoons, separated by a sand barrier, exchange water with the South

Table 2 Parameters of remote sensing images

Year	Date	Sensor type	Geometric resolution
1987	12/06	L5TM	30 m
1992	07/12	L5TM	30 m
1996	12/14	L7ETM+	15 m
2001	10/17	L7ETM+	15 m
2007	07/06	L5TM	30 m
2013	10/10	L8OLI	15 m
2013	10/26	L8OLI	15 m
2013	12/29	L8OLI	15 m

China Sea via two narrow inlets; conditions in the lagoons are controlled by the seasonal tropical wave action and relatively high sea temperatures, typhoon activity, and humidity. Rainfall is abundant in summer, but little precipitation falls in spring and autumn. Monkey Island and Niubai Hill are located to their south and serve as natural barriers.

In December 31, 2009, the Chinese government initiated a project to build an International Tourism Island that will include these two lagoons on Hainan Island.

Original data

The research data included multi-phrase images, land terrain surveying maps, bathymetric survey data, and tidal survey data (Table 1).

RS images in eight years from Landsat 5, 7, and 8 were gathered with three types of sensors, TM, ETM+, the Landsat Operational Land Imager (OLI), by the U.S. Geological Survey (Table 2). The Landsat 8 images included new Bands 1 and 9 that were applied during coastal observation and analysis.

Methodology

Tidal currents and waves control the formation of instantaneous shorelines of the lagoons. This study analyzed the long-term spatial evolutionary trends of these lagoons and their coastlines by extracting the shorelines of the lagoons at the moment when the satellite images were taken. The Water

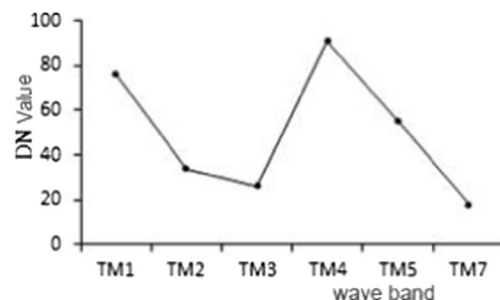


Fig. 2 Plant digital numbers (DN) value before radiometric correction

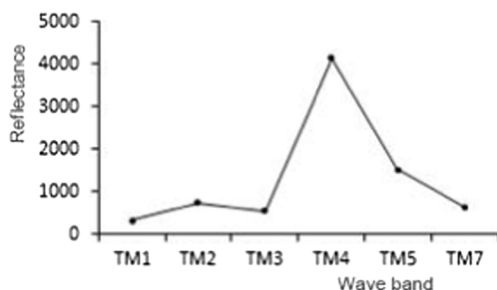


Fig. 3 Plant reflectance after radiometric correction

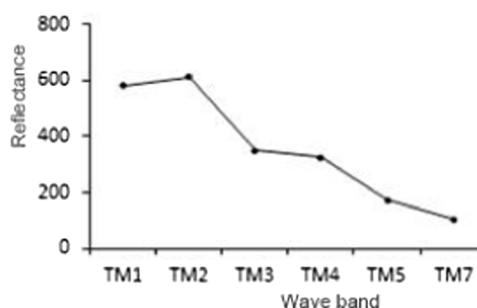


Fig. 5 Water reflectance after radiometric correction

Body Index method and ArcGIS spatial analysis were conducted together to obtain the average high-tide coastlines using a digital 3D terrain model of the tidal flats and tide correction. Then the instantaneous shorelines on the images were converted to their average high-tide coastlines using the Threshold Method of the Humidity Component and overlaying the spatio-temporal analysis.

Preprocessing of RS images

The image data from TM, ETM+, and OLI sensors, based on three different sensor types, released from the Landsat satellite ground station in the US were processed with geometric correction. The present research converted the Digital Number (DN), the initial value of surface reflection of electromagnetic waves, into the surface albedo by correcting reflection, followed by analyzing the spectral curve of the ground features. All images were processed using ENVI5.1 software, first by gaining the apparent atmospheric reflectance by both radiometric calibration and atmospheric correction.

Radiometric calibration

Radiometric calibrations were processed with two steps using the ENVI5.1 software after inputting latitude and longitude of the image center, imaging date, time, and other appropriate parameters: (1) convert the initial DN value into radiance brightness; (2) converting the radiance brightness value into atmospheric surface reflectance.

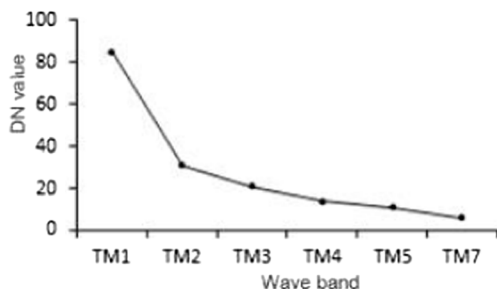


Fig. 4 Water digital numbers (DN) value before radiometric correction

Atmospheric correction

Atmospheric surface reflectance and radiance brightness can be obtained after the radiometric calibration. The present study first carefully analyzed the actual spectral profiles before extracting shorelines and interpreting RS images; then, landforms were classified to identify different spectra of ground features and to select an appropriate model and method of shoreline extraction and classification. Atmospheric correction of RS imagery was conducted to eliminate the errors caused by atmospheric scattering, absorption, and reflection, and to obtain the real physical quantity of land surface reflectance.

The present study included atmospheric correction of RS imagery through Fast Line-of-sight Atmospheric Analysis of Spectral Hypercubes, a calibration tool of the atmospheric correction module in ENVI 5.1 software. Using this type of software provides the most accurate way to remove the scattering effect of water vapor/aerosol efficiently by estimating atmospheric properties through the spectral characteristics of images to output real surface reflectance.

After atmospheric correction, the reflectance of water and typical plants were compared with *The Knowledge Database of Chinese Typical Objects* (a nationally certificated sample database for China). The atmospheric correction seemed to be successful as evidenced by the fact that the reflectance profile was close to the characteristics of the national database (Figs. 2, 3, 4, and 5) and satisfied the needs for general RS research and application.

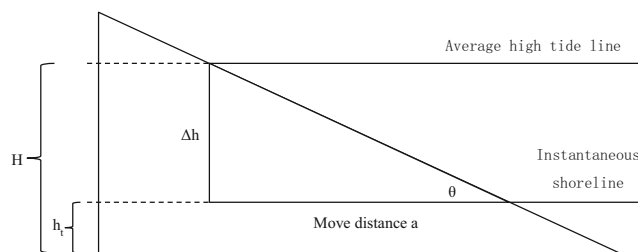


Fig. 6 The principle used to convert distance

Table 3 Tide level when satellite images were taken

No.	Date	Time	Instantaneous tide level h_t (m)		Average high-tide level H (m)	
			Xincui	Li'an	Xincui	Li'an
01	10/10	3:07:33	0.38	-0.02	0.67	0.42
02	10/26	3:07:25	0.44	0.03		
03	12/29	3:07:05	0.59	0.05		

Fig. 7 Method for calculating the average high-tide line

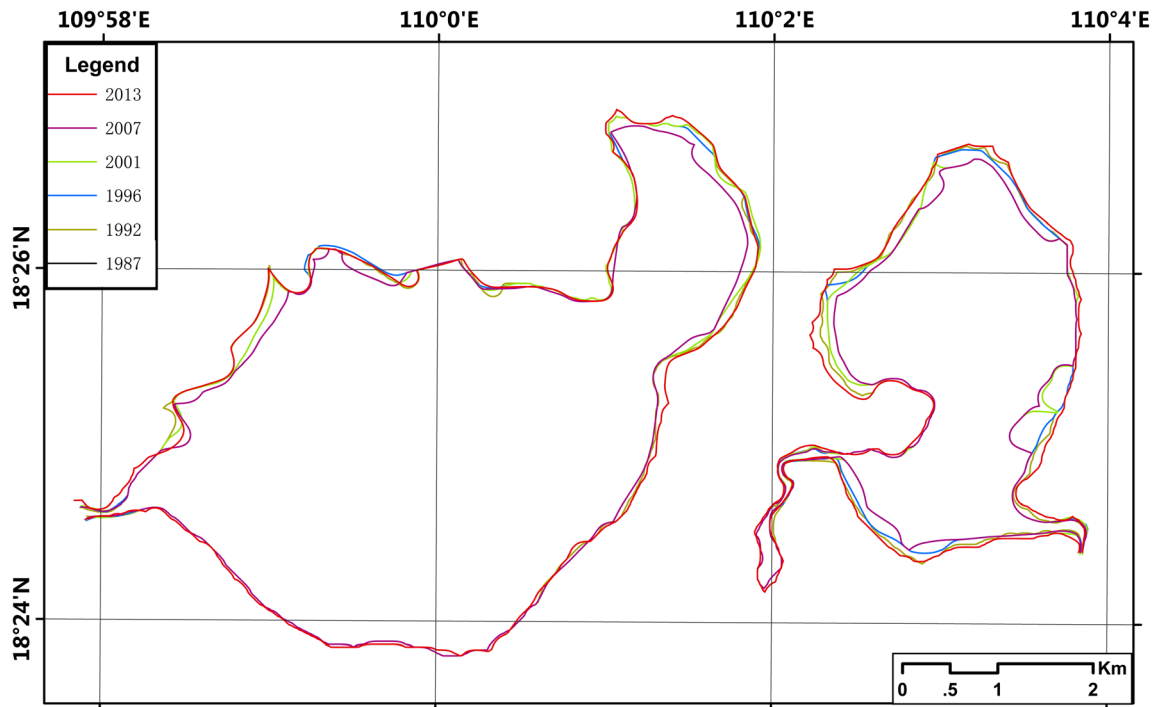
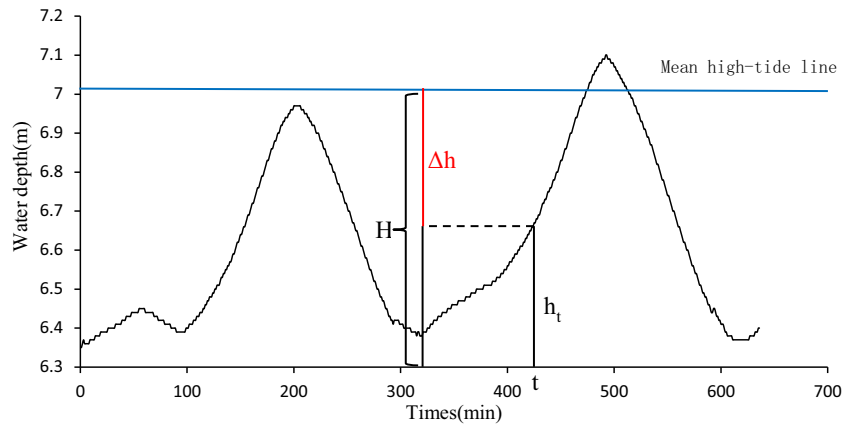


Fig. 8 The average high-tide along coastlines for 6-year periods from 1987 to 2013

Table 4 Changes in coastlines of Xincun and Li'an Lagoons from 1987 to 2013

Year	Total length		Artificial coastlines		Percentage of artificial coastlines	
	Xincun (km)	Li'an (km)	Xincun (km)	Li'an (km)	Xincun	Li'an
1987	24.71	19.88	4.92	0.36	19.90%	1.79%
1992	24.69	19.72	4.03	0.34	16.31%	1.75%
1996	24.30	19.26	9.70	4.05	39.93%	21.02%
2001	24.29	20.33	12.47	9.70	51.34%	47.73%
2007	24.13	19.99	11.57	10.09	47.94%	50.46%
2013	23.02	19.00	11.53	9.59	50.07%	50.47%

Modified normalized difference water index (MNDWI)

A Normalized Difference Water Index (NDWI) was used to develop a water index based on the multi-spectral variation rule and its relationship between water and the aquatic background by taking advantage of the abundant spectral information available in RS imagery.

In 1996, McFeeters (1996) proposed the NDWI that uses a widely applied method of analyzing a multi-spectral relationship to identify the difference between water and vegetation, although this method does not clearly distinguish between soil and buildings.

The Modified NDWI (MNDWI), proposed by Xu (2005), was constructed using the middle infrared bands (MIR from Landsat Thematic Mapper 5 imagery) instead of near infrared bands (from Landsat Thematic Mapper 4) to extract the water boundary of lagoons. Xu (2005) showed that the MNDWI can reveal subtle features of water more efficiently than the NDWI and can remove shadow noise from water information to allow researchers to tell the difference between water and vegetation as well as between water and buildings. Eq. (1) Provides the MNDWI formula (Xu 2005):

$$MNDWI = (Green - MIR) / (Green + MIR) \tag{1}$$

Where ‘Green’ is the green band, the second band of Landsat TM and ETM+ imagery, or the third band of OLI imagery; ‘MIR’ is the middle infrared band, the fifth band of TM, ETM+ and OLI imagery.

Tide correction

Tide correction should be processed after obtaining the water boundary through the MNDWI. Doing this requires the terrain of tidal flats and local tidal character based on the average high-tide height (H), the instant tide level (h_t) at the moment of the image obtained, coast slope (θ), and the distance a between instantaneous shoreline and average high-tide line to confirm the coastline location (Shen et al. 2009; Fig. 6).

The tide characteristics of the study area in 2013 and H were calculated by harmonic analysis based on surveying tide data. The tide level in each hour in 2013 was then simulated accurately through the harmonic constants and was used to calculate the instantaneous tide level and the average high-tide level when the satellite images were captured (Table 3).

The height difference (Δh) between the instantaneous shoreline and the average high-tide line on three OLI images was calculated according to the time (t) and h_t read from the harmonic curve (Fig. 7).

The coast slope θ' was calculated through the digital elevation model from a 2011 survey. The research delineated 20 sections in Xincun and 18 sections in Li'an. Each section was

Fig. 9 Coastline change and the distribution of man-made coastlines in Xincun Lagoon from 1987 to 2001

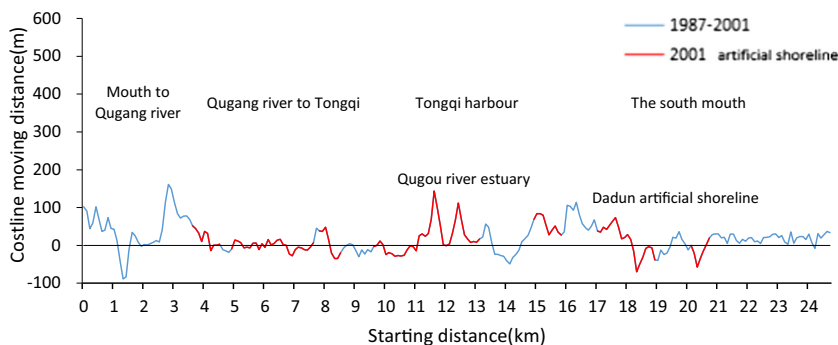


Fig. 10 Coastline change and the distribution of man-made coastlines in Xincun Lagoon from 2001 to 2013

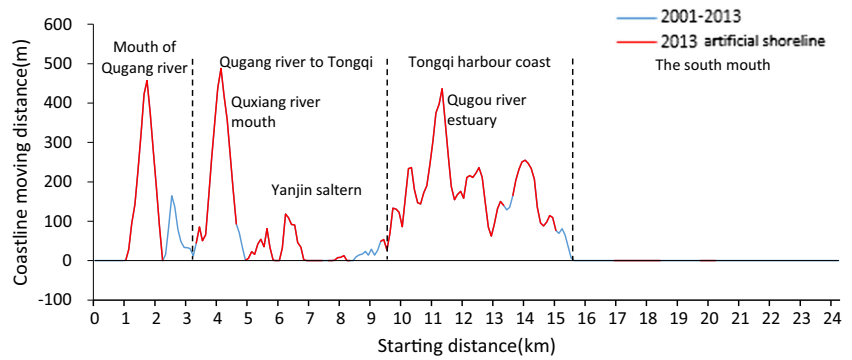
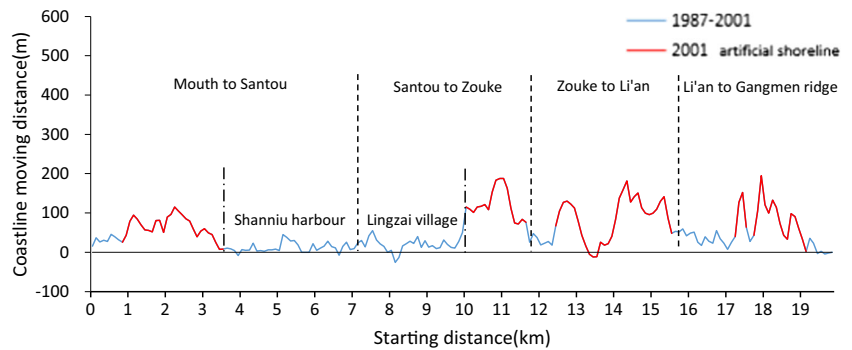


Fig. 11 Coastline change and the distribution of man-made coastlines in Li'an Lagoon from 1987 to 2001



composed of two survey points were chosen in the study, and the slope was calculated as:

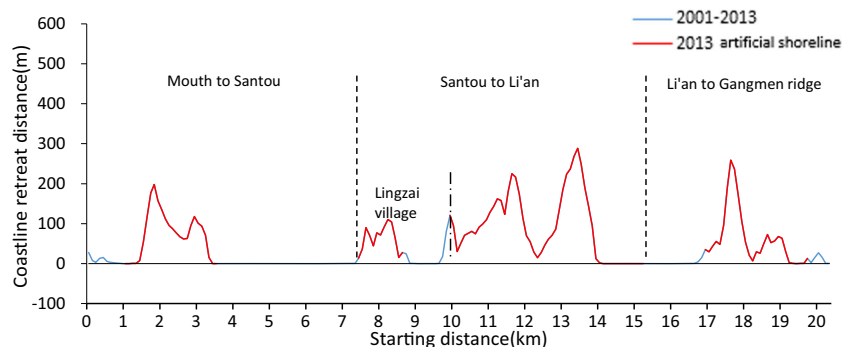
$$\tan\theta = \frac{\Delta h_1}{d} \tag{2}$$

Where d is the distance between two terrain points; Δh_1 is the height difference between two terrain points.

Finally, the distance correction of instantaneous shorelines (a), can be obtained from Δh , the tide difference between average high-tide line and instantaneous shoreline, and the average θ (Fig. 6):

$$a = \frac{\Delta h}{\tan\theta} \tag{3}$$

Fig. 12 Coastline change and the distribution of man-made coastlines in Li'an Lagoon from 2001 to 2013



Threshold method of determining the humidity component

K-T Transformation, proposed by Kauth and Thomas (1976), is typically used to extract the humidity component from a Landsat TM image. Commonly, a K-T matrix used with TM and ETM+ sensors is produced by the method of Crist (1985). Because Band 5 of Landsat 8 OLI eliminates the absorption characteristics of water vapor at 0.825 μm and narrows the scope of Band 8, the present study adopted a K-T matrix use with an OLI image as proposed by Baig et al. (2014) to extract humidity components from three-phase images in 2013. Next, RS images were divided into other different years through the obtained parameters of the average three humidity components to extract average high-tide lines.

Results

High-tide coastlines on RS images over a 26 year period

By combining K-T image processing and field surveying transformation methods, the instantaneous water boundary was extracted from historical RS images separately; next, the data were adjusted and converted to the average high-tide line of coastlines. The final average high-tide coastlines for 6 years in 1987–2013 are overlain in (Fig. 8).

Variation in length variation of coastlines of the two lagoons

The results show that salt fields, marine aquiculture, and inner-land culture activities around the lagoons have gradually increased from the beginning of the 1980s. The present study investigated the coastlines by field work and differentiated man-made coastlines from the natural one based on their usage pattern; the total length of man-made coastlines increased correspondingly to 50% by 2013 (Table 4, Figs. 9, 10, 11 and 12) while, the total length of coastlines shrank (Figs. 13 and 14).

Variations in the spatial position of coastlines

By stretching the coastlines into one-dimensional straight lines through samples taken every 100 m via ArcGIS software, the displacement of the coastlines

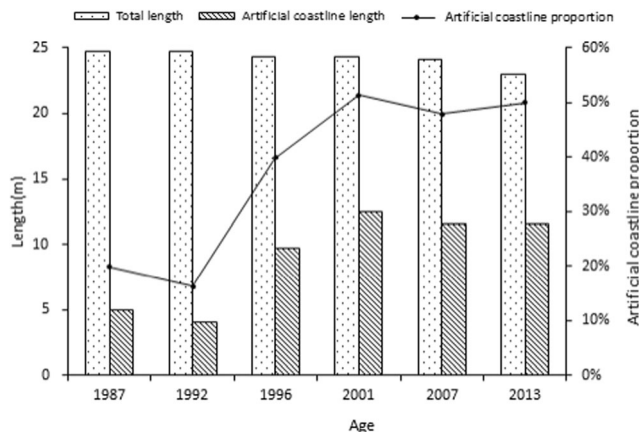


Fig. 13 Changes in the length of the coastlines of Xincun Lagoon from 1987 to 2013

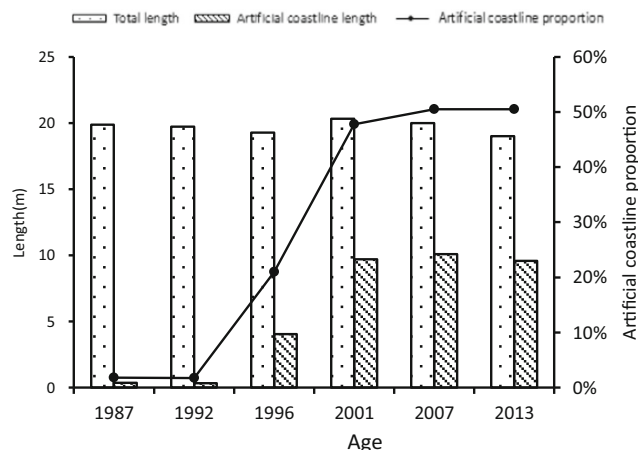


Fig. 14 Changes in the length of the coastlines of Li'an Lagoon from 1987 to 2013

was calculated and compared at each spatial position; in addition, the rate of movement and spatial range in two intervals (1987–2001 and 1987–2013) were determined. The x-axes in Figs. 15 and 16 represents the one dimensional coastline of each lagoon in different years, with Xincun starting at the north entrance and Li'an at the west entrance. The y-axis represents the seaward (positive value) or landward (negative) displacement, respectively, from the lagoon center. As these figures show, from 1987 to 2013 the general coastlines moved seaward by 94.04 m and 102.5 m at rates of 3.62 m and 3.94 m per year in Xincun and Li'an, respectively. The coastlines in Xincun slowly moved seaward by an average of 18.26 and 74.61 m at speeds of 1.3 m and 6.2 m per year from 1987 to 2001 and 2001–2013, respectively. However, the coastlines in Li'an moved seaward by an average of 52.08 and 48.14 m at speeds of 3.72 and 4.10 m per year between 1987 and 2001 and 2001–2013, respectively. In general, some parts of coastlines moved farther than the average rate, and as much as 400 m.

Meanwhile, the man-made coastlines in Xincun (Figs. 9 and 10) and Li'an (Figs. 11 and 12) Lagoons were becoming longer and moving seaward. Most of these man-made coastline was designed to create upland areas and their lengths increased sharply after 2001.

Area change in the two lagoons

The area of the two lagoons has decreased over 26 years with coastlines moving seaward continuously (Fig. 17). The area of Xincun Lagoon has decreased by 8.2% from 21.17 km² to 19.43 km² and Li'an has decreased by 20.3% from 9.94 km² to 7.92 km² (Fig. 18).

Fig. 15 Shifting of the Xincun Lagoon coastline from 1987 to 2013

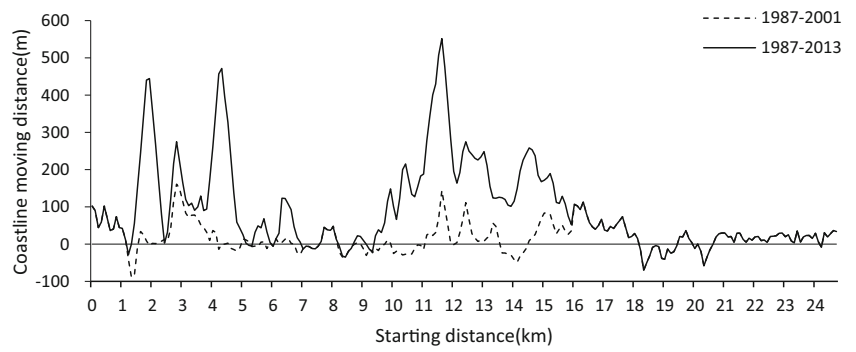


Fig. 16 Shifting of the Li'an Lagoon coastline from 1987 to 2013

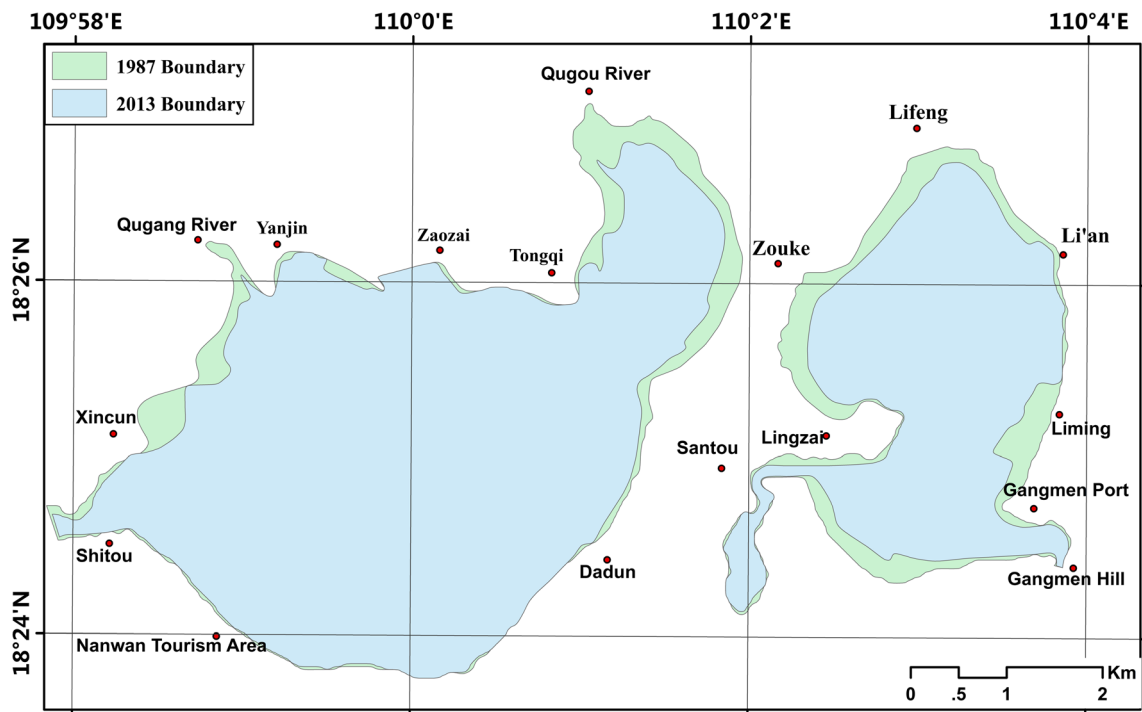
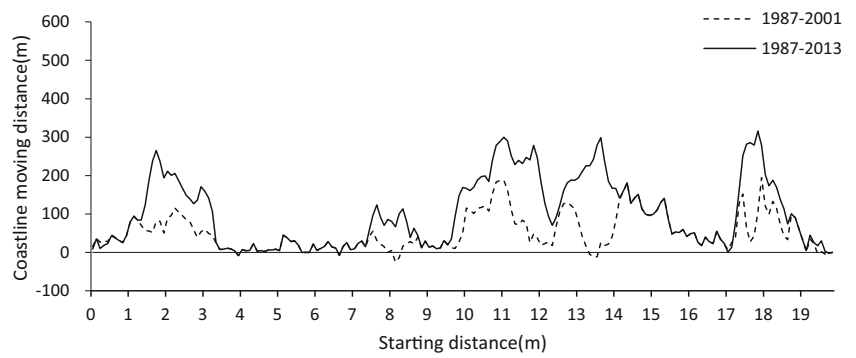
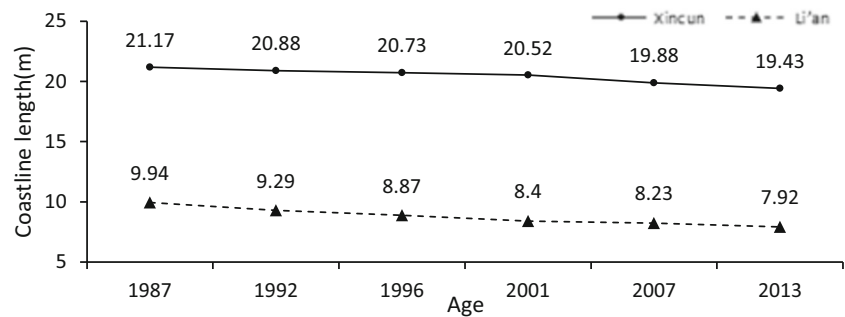


Fig. 17 Changes in area of Xincun and Li'an Lagoons from 1987 to 2013

Fig. 18 Changes in length of coastlines of Xincun and Li'an lagoons from 1987 to 2013



Discussion

Technology used in the present study was entirely based on Landsat RS images because these provide long-term data resources. In the future, other contemporary high-resolution RS images should be used for further analysis of geomorphological and human impacts. Meanwhile, more detailed reasons for what generated the increase in man-made coastlines and why the length of the lagoons' coastlines has declined should be investigated and analyzed in an upcoming project research study known as the Environmental Carrying Capacity and Green Development in Lingshui County with integrated analysis of geomorphology, hydrodynamic forces and sedimentology through the prospective use of SCHISM modeling (Zhang et al. 2016). The development of sustainable management policies will be analyzed during the next research study.

Conclusion

The present study developed a new technology-based method of deriving historic coastlines from corresponding RS images through their humidity component as processed by K-T Transformation Methods. The latest coastlines were derived with MNDWI methods that combine the survey data on tides and tidal-flat elevation. This method overcame the barriers created by a scarcity of historic tidal-level data and allowed us to effectively calculate historic coastlines and to evaluate the long-term movement of coastlines.

Through spatial and statistical analysis for six specific years from 1987 to 2013, the present study revealed that the man-made coastlines of Xincun and Li'an Lagoons grew by 47.94 and 50.46%, respectively, and the coastlines moved seaward by 94.04 and 102.56 m, respectively. The area covered by Xincun has decreased from 21.17 to 19.43 km² (−8.2%), and the area of Li'an decreased from 9.94 to 7.92 km² (−20.3%). Excessive anthropogenic activity, such as salt-field development, marine aquaculture, and

land reclamation for aquaculture ponds (mainly for shrimp and fish), are the main causes of the amount of pressure on the environment, as the shorter coastlines of the lagoons caused the lagoon area to shrink, led to a reduction in their storage capacity for tidal water, and limited the water exchange, all of which would in turn induce red tides, flooding and other natural disasters.

Acknowledgements The authors gratefully acknowledge financial support from the China Scholarship Council, funding for two Hainan governmental projects of Research on Environmental Carrying Capacity and Green Development in Lingshui County, Hainan Province and from the Study on Geomorphic-Dynamic of Tidal Inlets and Connecting Location of Two Lagoons in the Hainan International Tourism Island Pilot Zone. The authors also want to thank four anonymous reviewers for their helpful comments on the manuscript.

References

- Anthony EJ, Blivi AB (1999) Morphosedimentary evolution of a delta-sourced, drift-aligned sand barrier-lagoon complex, western bight of Benin. *Mar Geol* 158(1–4):161–176
- Baig MHA, Zhang L, Shuai T, Tong Q (2014) Derivation of a tasseled cap transformation based on Landsat 8 at-satellite reflectance. *Remote Sens Lett* 5(5):423–431
- Chinese Compilation Committee of Embayment (1999) Records of China Bays. Ocean Press, Beijing, pp 1–426
- Crist EP (1985) A TM tasseled cap equivalent transformation for reflectance factor data. *Remote Sens Environ* 17(3):301–306
- Feng C, Hui-Mei C, Xian-Ze S, Dong-Xing X (2007) Analysis on morphodynamics of sandy beaches in South China. *J Coast Res* 231:236–246
- Frihy OE, Dewidar KM, Nasr SM, El Raey MM (1998) Change detection of the northeastern Nile Delta of Egypt: shoreline changes, spit evolution, margin changes of Manzala lagoon and its islands. *Int J Remote Sens* 19(10):1901–1912
- Gao S, Collins M (1994) Tidal inlet equilibrium, in relation to cross-sectional area and sediment transport patterns. *Estuar Coast Shelf Sci* 38(2):157–172
- Gao S, Zhou L, Li G, Wang D, Yang Y, Dai C, Han Z, Wang H, Tu J, Yang B (2016) Processes and sedimentary records for Holocene coastal environmental changes, Hainan Island: an overview. *Quat Sci* 36(1):1–17

- Jia PH, Xia Z, Yin Y, Xue Q (2016) Lingdingyang Bay, Pearl River Estuary (China): geomorphological evolution and hydrodynamics. *Geol Soc London* 429:171–184
- Kauth R J, Thomas G S (1976) The tasseled cap—a graphic description of the spectral-temporal development of agricultural crops as seen by Landsat. *Proceedings of the Symposium on Machine Processing of Remotely Sensed Data*, Purdue University of West Lafayette, Indiana, 4B:41–51
- Li X, Zhang L, Ji C (2014) Spatio-temporal changes of Jiangsu coastline: a remote sensing and GIS approach. *Geographical Research* 33(3): 414–426
- Liu YX, Li MC, Zhou MX, Yang K, Mao L (2013) Quantitative analysis of the waterline method for topographical mapping of tidal flats: a case study in the Dongsha Sandbank, China. *Remote Sens* 5:6138–6158
- McFeeters SK (1996) The use of the normalized difference water index (NDWI) in the delineation of open water features. *Int J Remote Sens* 17(7):1425–1432
- Ryu JH, Won JS, Min KD (2002) Waterline extraction from Landsat TM data in a tidal flat: a case study in Gomsu Bay, Korea. *Remote Sens Environ* 83(3):442–456
- Shen J, Zhai J, Guo HT (2009) Study on coastline extraction technology. *Hydrographic Surveying and Charting* 29(6):74–77
- Wang Y, Wang Q, Zhan C, Wang L, Zhang M (2013) Changes in coastline and deposition/erosion pattern of Rushan Bay, Jiaodong Peninsula, China under the influence of human activities in recent 40 years. *Mar Geol Quat Geol* 33(2):41–50
- Xu H (2005) A study on information extraction of water body with the modified normalized difference water index [J]. *J Remote Sens* 5: 589–595
- Zhang Y, Ye F, Stanev EV, Grashorn S (2016) Seamless cross-scale modeling with SCHISM. *Ocean Model* 102:64–81